Supporting information

Vertically aligned graphitic carbon nanosheet arrays fabricated from graphene oxides for supercapacitors and Li–O_2 batteries

Guangyu Zhao, Li Zhang, Jixian Lv, Changle Li, Kening Sun*

Academy of Fundamental and Interdisciplinary Sciences, Harbin Institute of Technology, Harbin, China. E-mail: keningsunhit@126.com (K. Sun).

Experimental section

Preparation of VAGN films

All the reagents in the experiments were analytical pure. Graphite oxide was prepared by oxidizing graphite using the improved Hummers method. The graphite oxide product was suspended in distilled water to give a viscous, brown, 4 mg mL^{-1} dispersion, which was subjected to dialysis to completely remove metal ions and acids. Graphene oxides (GOs) were prepared by treating the as-prepared graphite oxide with ultrasonic in diluted solution. The ammonium peroxo-polymolybdate solution was prepared by dissolving 3.0 g Mo powder (2 μm, Aladdin Chemistry) in 100 mL H_2O_2 at 60 °C following the reactions:

$$2Mo+10H_2O_2 \rightarrow Mo_2O_{11}^{2-}+2H^+ +9H_2O \quad (1)$$

When the metal powder was completely dissolved and the exothermic reaction had ended, a Pt foil was added to reduce the excess peroxide. Then the solution was neutralized to be neutral with ammonia. In a typical hydrothermal procedure, 1.0 mL GO suspension was mixed with 0.065 mL $(NH_4)_2Mo_2O_{11}$ aqueous solution (30.0 mg

23 mL^{-1}) (the mass ratio of $(NH_4)_2Mo_2O_{11}$ to GO was 1:2), and the mixture was diluted
24 to 80 mL with deionized water. Then the mixture was treated by ultrasound 0.5 h to
25 disperse the GOs. Other mass ratios were achieved by adjusted the amount of
26 $(NH_4)_2Mo_2O_{11}$. Then a circular Ni foam plate (diameter = 15 mm) was dipped in the
27 mixture. The mixture was sealed in a Teflon-lined stainless steel autoclave and
28 maintained at 180 °C for 16 h; the as-obtained Ni foams were naturally cooled to
29 room temperature followed by freeze-drying. The dry samples were heat-treated at
30 350 °C for 3 h in Ar atmosphere to lead a crystallization of molybdenum dioxide. The
31 weights of as-prepared VAGN films were measured by means of a micro-balance
32 (Mettler Toledo, USA) with an accuracy of 0.01 mg. The weight of the films was
33 around several mg.

34 *Supercapacitor and Li–O_2 battery tests*

35 For supercapacitive measurement, a three electrode cell was used for all
36 electrochemical measurements. A VAGN film electrode was vertically inserted into
37 the electrolyte and acted as the working electrode, a Pt plane acted as the counter
38 electrode, and a SCE acted as the reference electrode. Cyclic voltammogram (CV)
39 and electrochemical impedance spectra (EIS) measurements were performed using a
40 CHI 660D with Na_2SO_4 solution (1.0 M) as the electrolyte. The Li–O_2 batteries were
41 measured in Swagelok type models assembled inside an MBraun glove box. The cells
42 were constructed by placing a 15 mm diameter Li disk on the bottom, covering it with
43 a piece of glass fiber separator (20 mm diameter, Whatman), adding excessive
44 electrolyte (1.0 M LiTFSI in tetraethylene glycol dimethyl ether (TEGDME)), placing

an VAGN coated Ni foam on the separator, and sealing the Swagelok cell. All the electrochemical measurements to the batteries were carried out in pure O_2 at 1 atm (99.99%). A BTS-2000 Neware Battery Testing System was employed for charge/discharge tests. CV measurements were also performed using the CHI 660D.

Instruments for Characterization

Scanning electron microscope (SEM) images were obtained on a Hitachi Su-8100. The X-ray diffraction (XRD) patterns were obtained on a PANalytical X´pert PRO X-ray diffractometer with Cu Kα radiation (λ = 1.5418 Å). High resolution transmission electron microscope (HRTEM) images, selected area electron diffraction (SAED) and energy dispersive X-ray spectrum (EDS) patterns were obtained on a FEI Tecnai G^2. X-ray photoelectron spectra (XPS) were obtained with a K-Alpha electron spectrometer (Thermofish Scientific Company) using Al Kα (1486.6 eV) radiation. The base pressure was about 1×10^{-8} mbar. The binding energies were referenced to the C1s line at 284.8 eV from adventitious carbon.

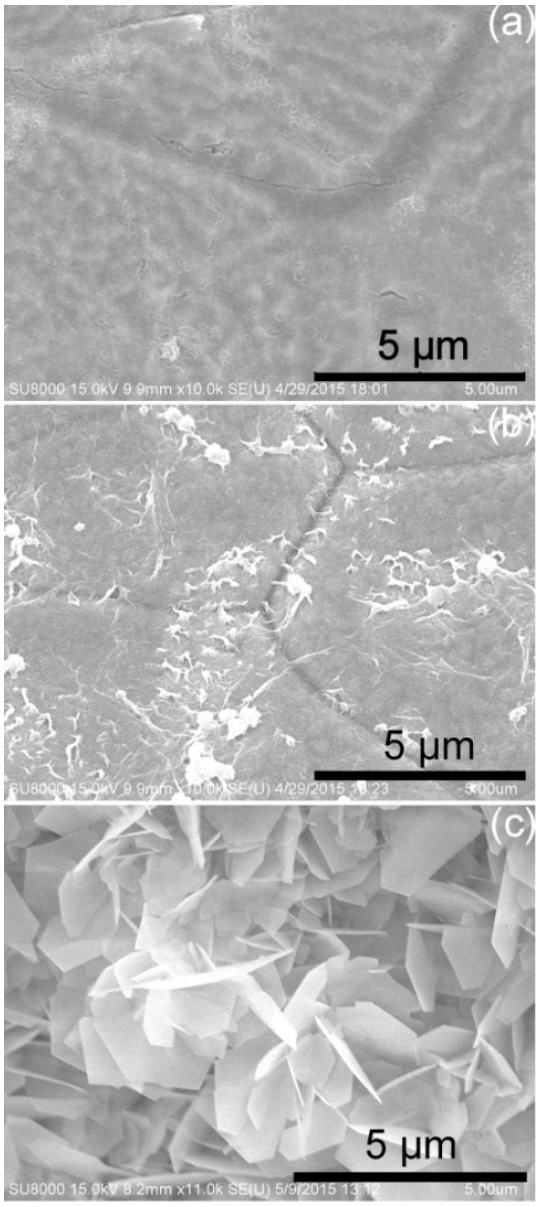

Fig. S1. SEM images of Ni surface after hydrothermal treatment in GOs with different salts: (a) $NiCl_2$, (b) $Co(NO_3)_2$, (c) $Fe(NO_3)_3$. Rates of charge for the three experiments all are salt: GO = 1:1 in weight.

Explanation: No VAGN can be detected on Ni foams treated in the three solutions. GOs lying on Ni surface in Fig. S1b have a size consistent with pristine GOs, and the hexagonal flakes in Fig. S1c are not graphitic sheets. These all indicate the three salts have not interaction with GOs.

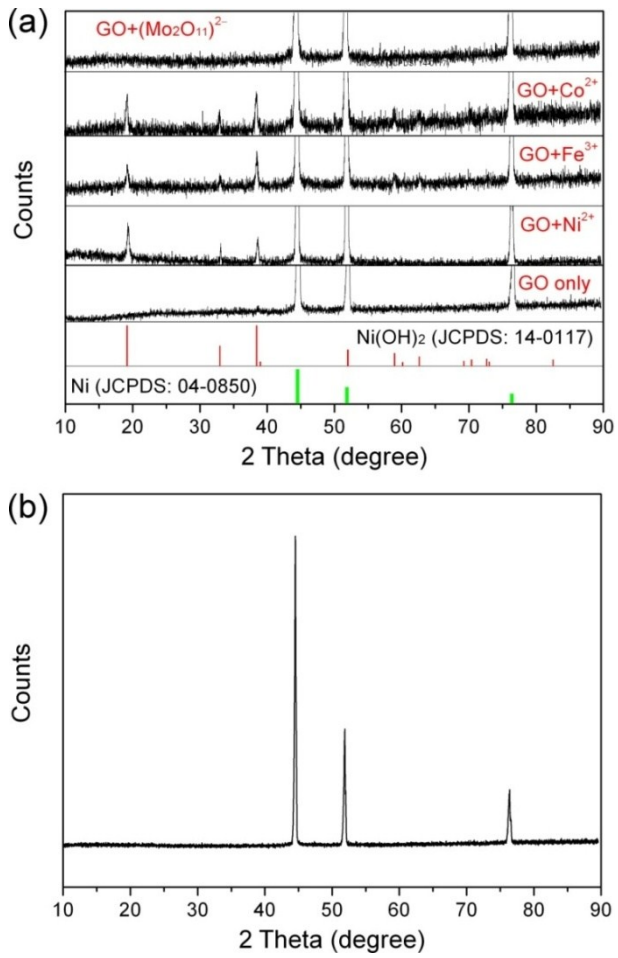

Fig. S2. XRD patterns of Ni foams treated with different solutions in hydrothermal synthesis: (a) in GOs, GOs+ $NiCl_2$, GOs+ $Fe(NO_3)_3$, GOs+$Co(NO_3)_2$ and GOs+$(NH_4)_2Mo_2O_{11}$; (b) in $(NH_4)_2Mo_2O_{11}$ solution without GOs.

Explanation: The Ni foams from hydrothermal reactions with GO-containing solutions of Ni^{2+}, Fe^{3+} or Co^{2+} all present $Ni(OH)_2$ patterns (JCPDS: 14-0117). The XRD pattern of Ni foam from "GO only" solution has no obvious variation compared with raw Ni foam, demonstrating no interaction of GOs with Ni foam. However, Ni foam covered with VAGNs from the $Mo_2O_{11}^{2-}$-containing GO solution also exhibits no variation. Otherwise, XRD result of Ni foam treated in the $(NH_4)_2Mo_2O_{11}$ solution only (no GOs) also exhibits the pattern of Ni metal (JCPDS: 04-0805), as shown in Fig. S2b. The XRD results reveal $Mo_2O_{11}^{2-}$ can react with GOs but not with Ni foam.

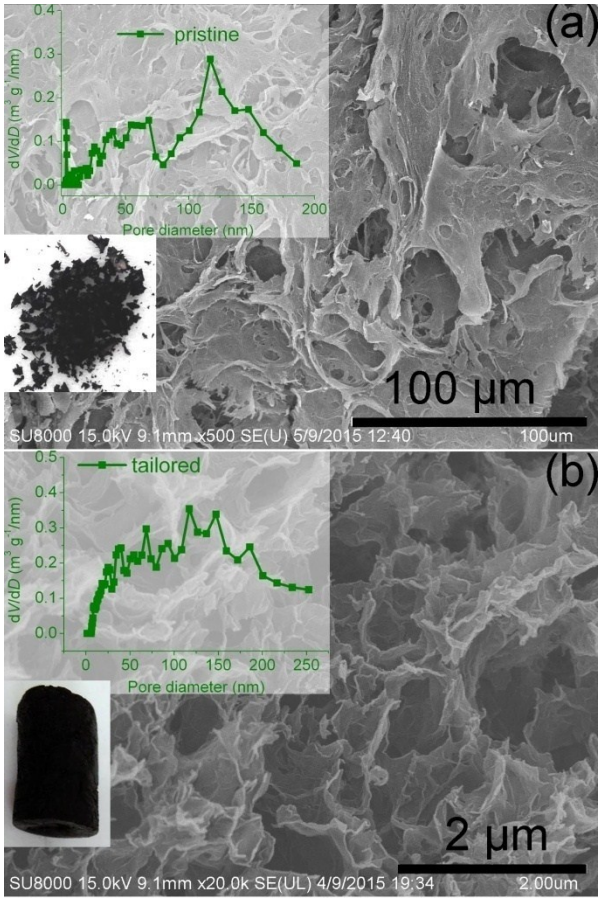

Fig. S3. SEM images of the products (no Ni foam) from hydrothermal in GOs only and GOs+$(NH_4)_2Mo_2O_{11}$ (rate of charge is 1:1). Upper left insets are corresponding pore size distribution curves and left down insets are corresponding digital photographs of the products.

Explanation: The graphitic sheets align to form porous cylinder foam from the solution of GOs+$(NH_4)_2Mo_2O_{11}$, compared with the powder obtained from GOs only, as shown in the digital photographs in left bottom of Fig. S3a and b. Apparently, $Mo_2O_{11}^{2-}$ anions can tailor graphitic sheets to be much smaller (Fig. S3b) resulting in smaller pore size of the foam, which can be verified by the pore size distribution curves in upper left of Fig. S3a and b.

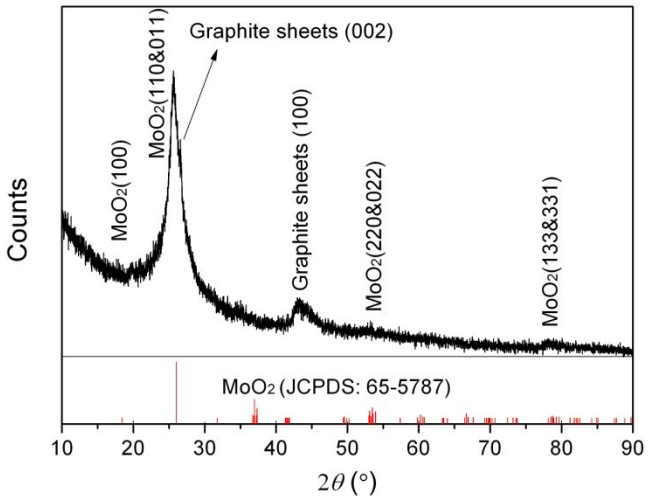

91

92 Fig. S4. XRD pattern of the powder scraped from VAGN films.

93 Explanation: The graphite (002) demonstrates GOs stacking in VAGN films, and the

94 other peaks can be ascribed to MoO_2 (JCPDS: 65-5787).

95

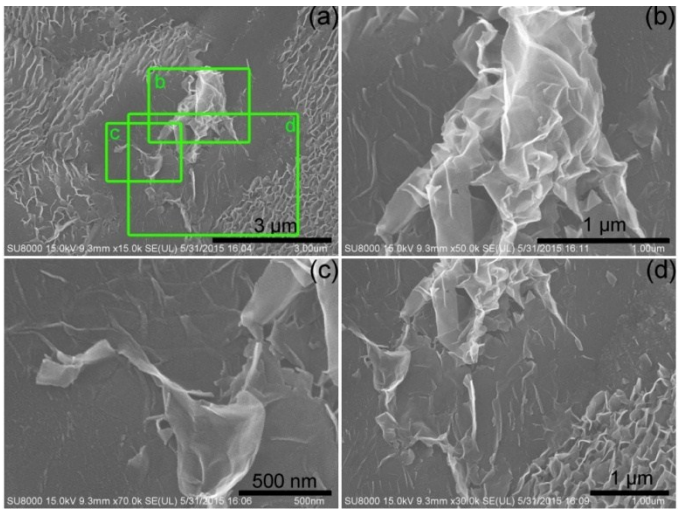

96

97 Fig. S5. SEM images of a special case that GO aggregate and VAGNs coexisting (1:2

98 rate): (a) overview; (b, c, d) images corresponding to the square s in green squares in

99 (a).

100 Explanation: Fig. S5a is an overview, and b, c, and d are parts of a. The raw GO in

101 Fig. S5b lying on the Ni surface results in an area without "planted'' VAGNs. On the

102 other hand, some GO pieces are tailored from edges of the large pieces, and some of

them are stood on the Ni surface, as shown in Fig. S5c and d. Fig.S5 reveals that the tailoring of GO to smaller sized pieces is crucial for planting them onto the Ni substrates.

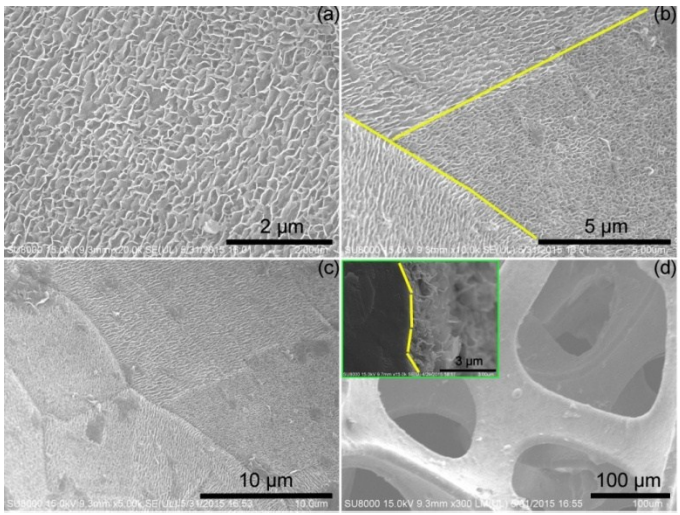

Fig. S6. SEM images in different magnifications of VAGN films (1:2 rate), the inset in (d) is profile view of the VAGN film.

Explanation: The typical surface morphology of the samples formed with a 1 : 2 ratio is presented in Fig. S6. Apparently, the nanosheets distribute on the Ni foam surface homogeneously, and rare GO aggregates disturb the good continuity. Notably, the VAGNs on different Ni grains have different orientations, causing visible boundaries between different areas, as shown in Fig. S6b and c. We suggest the interaction of MoO_2 and Ni, depending on the crystal orientation of surface Ni atoms, is responsible for the different orientations of the nanosheets. Fig. S6d shows the low magnification front view and profile view (inset) of the VAGN film (1 : 2 ratio). Obviously, the film is a single layer of nanosheets freestanding on the Ni surface.

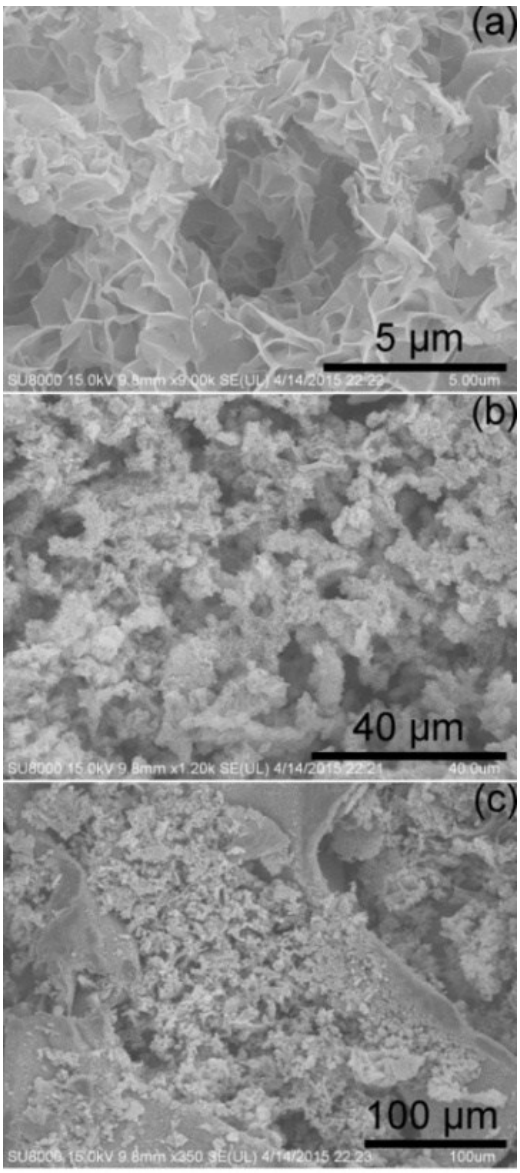

Fig. S7. SEM images in different magnifications of the products obtained from the rate of charge at 5:1.

Explanation: As the addition ratio rises to 5 : 1 (Fig. S7), a graphitic foam fills in the pores of the Ni foam owing to the continuous connection of GO fragments. Furthermore, the sizes of the graphitic sheets and pores in the foam obtained from a 5 : 1 ratio are all larger than the VAGN film obtained from the 1 : 2 ratio.

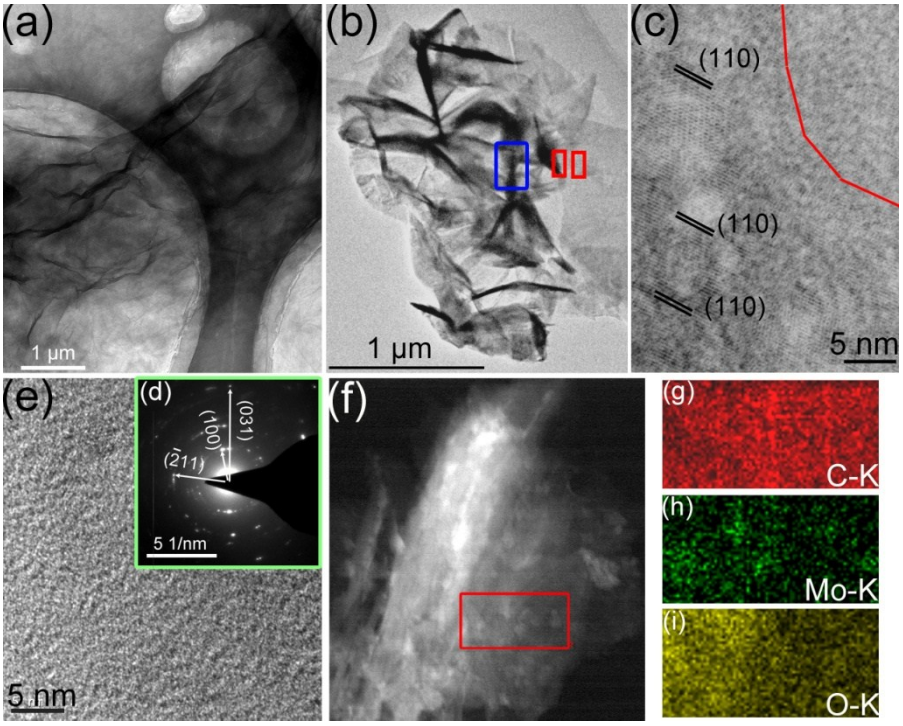

Fig. S8. TEM results of GOs and graphitic sheets scraped from Ni foams those treated by hydrothermal in 1:2 rate: (a) TEM image of pristine GOs; (b) TEM image of graphitic sheets scraped from Ni substrates; (c, e) High resolution TEM images of the area from the red square in c; (d) SAED pattern of the nanosheet; (f) STEM image of the dark area in a typical graphitic sheet from blue square in (b); (g, h, i) C, Mo, O EDS mapping of the selected area in the red box in (f).

Explanation: The tailoring process carries out at the defects of GOs, resulting in the MoO_2 generating on the edges of graphitic fragments, as shown in Fig. 2. The random motion of the fragments in hydrothermal synthesis leads the MoO_2 anchoring on Ni surface, resulting in the VAGN film forming in a self-assembly manner. The distribution of the three elements demonstrates that the MoO_2 act as "soil" when the "graphitic sheets plant" is anchored on the substrate.

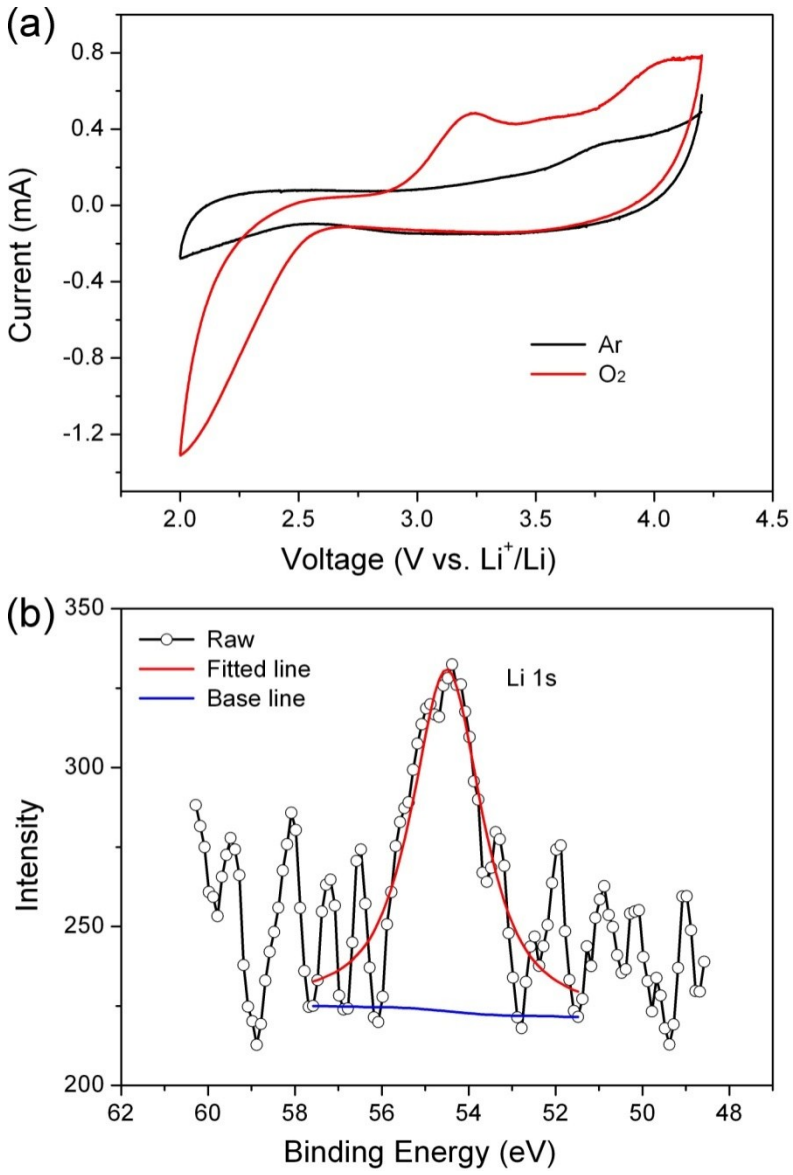

Fig. S9. (a) CV curves of the battery filled with Ar and O_2. (b) Li1s of the VAGN films after discharge in Li–O_2 battery.

Explanation: Fig. S9a shows the cyclic voltammograms (CV) of graphitic foam as cathode in a typical Li–O_2 battery. A clear distinction between ORR/OER and the argon background (black curve) is observed. Otherwise, XPS of Li1s from VAGN film after the 1st discharge in Fig. S9b reveals the generation of Li_2O_2 (54.3 eV), based on the previous result on the discharged sample using the same electrolyte.